

Design Study of Adhesively Bonded Structures

Jacung Chung*

ABSTRACT

The failure responses of adhesively bonded, hat stiffened structures are studied through numerical analysis using the finite element method. The responses are evaluated numerically for the bonded hat section/substrate structures containing different combinations of materials. It is studied what kind of material combinations causes the easier crack initiation in the structure. This study is conducted under plane strain conditions and J-integral via a commercial code ABAQUS as a total critical energy release criterion was used for observation on crack initiation. Also, the influence of adhesive on the structure is studied.

Key words : J-integral, Failure response, Adhesive, Crack initiation, Plane strain, Critical energy release criterion

1. Introduction

Composite materials are high strength to weight and cost effective materials. For these characters of the composite materials, the materials are increasingly used in the automotive and aerospace industries. When the materials are used in the mechanical structures such as vehicles, aircrafts and spacecrafts, the adhesive materials are utilized to assemble the composite materials instead of the traditional methods like bolt assembling or welding. When these adhesive materials are used to bond the composite materials, several problems are appeared to trouble to design the safe and reliable mechanical structures. One of the problems is the crack initiation between the adhesive and composite materials.

A lot of researches related to this problem are carried out. Fernlund and Spelt^[1] developed the fracture testing jig to investigate the entire mode-ratio range from pure mode I to pure mode II using the double-cantilever-beam specimens. They^[2] also calculated the strain energy release rate of cracked adhesive joints. A semi-infinite interface crack between two infinite isotropic layers was analytically solved by Suo and Hutchinson^[3]. Suo *et al.*^[4] studied the fracture behav-

ior of composite laminates analytically. Alternate and new numerical schemes to evaluate energy release rates has been proposed by Shen, Lee and Tay^[5]. They introduced a robust finite element based technique to compute the energy release rates based on the virtual crack closure technique (VCCT). The VCCT is an approximate method derived from the more fundamental crack closure technique (CCT)^[6,7]. Tay *et al.*^[8] showed that the distributions of energy release rate (as a function of crack length) calculated using CCT and VCCT are similar. Also, the VCCT is verified through experiments for adhesively bonded, hat stiffened structures^[9]. Reeder and Crews^[10] developed a mixed-mode delamination test procedure using a split unidirectional laminate.

In the present paper, what kind of material combinations causes the easier crack initiation in adhesively bonded, hat stiffened structures. This is performed through the failure mechanism of the structures using J-integral via ABAQUS.

2. Numerical Analysis

In this section, the material properties are presented for the numerical analysis to study the failure response of adhesively bonded, hat stiffened structures. And the validity of J-integral used in this study is confirmed through the comparisons among J-integral, VCCT and the analytical solutions derived by Suo *et al.*^[4] and Williams^[11]. Also, the numerical

*교신저자, 정회원, 경원대학교 기계자동차공학과
- 논문투고일: 2008. 03. 21
- 논문수정일: 2008. 12. 31
- 심사완료일: 2009. 01. 15

modeling is described for the numerical analysis to study the failure response of adhesively bonded, hat stiffened structures.

2.1 Material Properties

Material properties of *DOW MM 364* composite^[12] are expressed in Equation (1).

$$\sigma_{ij} = D_{ijkl} \epsilon_{kl} \tag{1}$$

where,

$$D_{ijkl} = \begin{bmatrix} 9082.7 & 2504.9 & 1505.9 & 66.2 & 148.0 & 701.6 \\ & 10827.0 & 1652.2 & 263.1 & 72.8 & 429.0 \\ & & 4666.9 & 61.6 & 138.9 & 218.2 \\ & & & 1317.3 & 2.4 & 11.2 \\ & symm. & & & 1432.9 & 14.1 \\ & & & & & 4000.8 \end{bmatrix} \text{MPa}$$

Material properties of Steel 1008^[13] are $E=207\text{GPa}$, $\nu=0.285$. Material properties of Aluminum 5052 Alloy^[14] are $E=78.280\text{GPa}$, $\nu=0.33$.

To obtain material properties of B. F. Goodrich Epoxy Adhesive, 5 tensile tests and 4 torsional tests were performed using a tensile test machine and a torsion test machine, respectively. One of the specimens had much more air bubbles than the others. This specimen will be referred to as specimen F.

Table 1. Design values for B. F. Goodrich epoxy adhesive

	Ultimate strain (%)	Strength (MPa)	Young's Modulus (GPa)	Poisson's Ratio
Specimen A	1.1	32	3.401	0.31
Specimen B	1.1	34	4.399	0.31
Specimen C	1.3	40	3.699	0.35
Specimen D	1.0	33	3.800	0.36
Specimen E	1.2	35	3.301	0.38
Average	1.1	35	3.720	0.34

Tensile test results are shown in Table 1, Fig. 1 and Fig. 2. The uniaxial tensile stress-strain curves for B. F. Goodrich Epoxy Adhesive are shown in Fig. 1.

As seen in Fig. 1, the material curves of 5 test specimens are reasonably consistent. Through this Fig., it is clear that the air bubbles in the specimens did not influence the material response too much. In Table 1, the tensile test results are summarized. Two strain gauges were installed on the specimen to obtain strains and Poisson's ratio of the adhesive material.

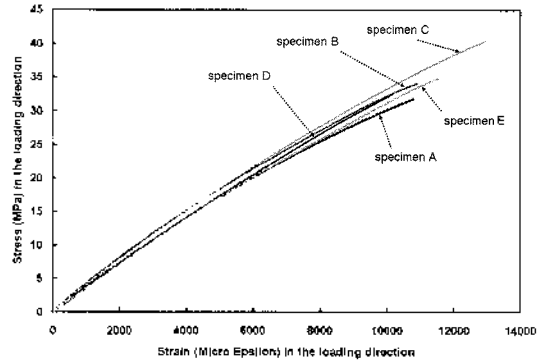


Fig. 1. The uniaxial tensile stress-strain curve for B. F. Goodrich epoxy adhesive.

Fig. 2 shows Poisson's ratio-strain (in the loading direction) curves for the adhesive material. As seen in Fig. 2, Poisson's ratio of each specimen converges to a certain value with increase of strain in the loading direction. The converged values of Poisson's ratio are summarized in Table 1. Torsion test results are shown in Table 2. As seen in Table 2, shear moduli of B. F. Goodrich Epoxy Adhesive obtained from 4 torsional tests are summarized.

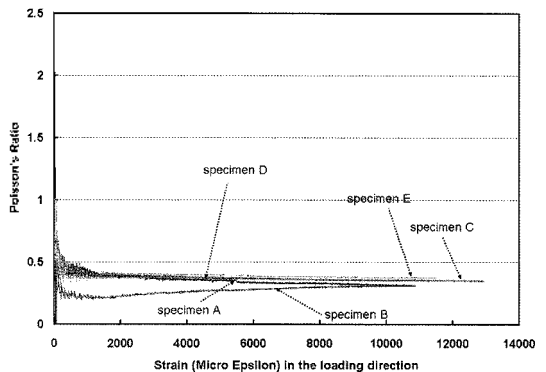


Fig. 2. The poisson's ratio-strain curve for B. F. Goodrich Adhesive.

Table 2. Shear modulus for B. F. Goodrich epoxy adhesive

Tested Shear Modulus (GPa)		Shear Modulus calculated through equation (2) (GPa)	
Specimen 1	1.254	Specimen A	1.298
Specimen 2	1.261	Specimen B	1.679
Specimen 3	1.357	Specimen C	1.370
Specimen 4	1.385	Specimen D	1.397
-	-	Specimen E	1.196
Average	1.314	Average	1.388

In addition, the obtained shear moduli are compared with the shear moduli calculated through substituting Young's moduli and Poisson's ratios which were obtained from 5 tensile tests via the equation (2).

$$G = \frac{E}{2(1+\nu)} \quad (2)$$

The shear moduli we obtained are reasonably close to the shear moduli calculated through using Young's moduli and Poisson's ratios of tensile tests. From the above experimental observation, it is concluded that B. F. Goodrich Epoxy Adhesive behavior is isotropic in the elastic regime. In order to check whether B. F. Goodrich Epoxy Adhesive is an isotropic material in the plastic regime, the following equations describing the uniaxial stress-strain response can be used.

$$\epsilon = \frac{\sigma}{E} + \left(\frac{\sigma}{B}\right)^n \quad (3)$$

where, n and B are obtained from tensile tests.

$$\gamma = \frac{\tau}{G} + \left(\frac{\tau}{A}\right)^n \quad (4)$$

where, $A = \frac{B}{3^{\frac{1}{2} + \frac{1}{2n}}}$

These equations are consistent and are applicable to a solid obeying J_2 deformation theory of plasticity. They are also identical to the equation for a solid obeying J_2 incremental theory of plasticity under proportional loading condition. Thus, if B. F. Goodrich Epoxy Adhesive is an isotropic material in the elastic and plastic regimes, the shear strain-stress curve

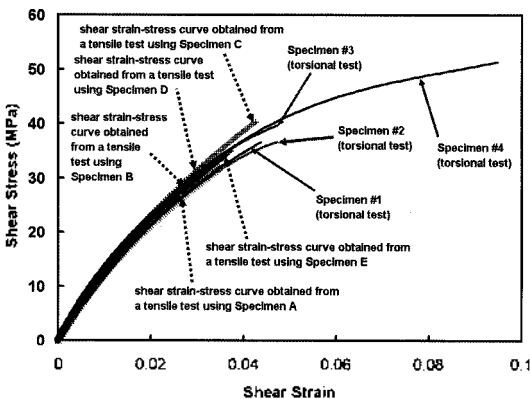


Fig. 3. Geometry of mixed mode end-loaded-split.

obtained through equation (4) and the data from tensile tests (B and n obtained from equation (3)) must be reasonably close to the shear strain-stress curve deduced from torsional test data.

As seen in Fig. 3, the shear strain-stress curves (thick dashed lines) are reasonably close to the shear strain-stress curves (thin straight lines) obtained from torsional tests. From the above experimental observation, it is concluded that B. F. Goodrich Epoxy Adhesive behavior is isotropic in the elastic and plastic regimes.

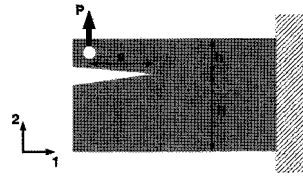


Fig. 4. Geometry of mixed mode end-loaded-split.

2.2 Validity of J-integral

Suo *et al.*^[4] derived the energy release rate (G) for the mixed mode End-Loaded-Split configuration of a composite laminate (see Fig. 4). They partitioned the total energy release rate, G into G_I (mode I energy release rate) and G_{II} (mode II energy release rate). The energy release rates analytically derived by Suo *et al.*^[4] are equation (5), (6), (7).

$$G = \frac{6(Pa)^2}{E_1 h^3} \left[1 - \left(1 + \frac{1}{\eta}\right)^{-3} \right] \left[1 + Y(\rho)(1 + F(\rho)(1 - \eta))\lambda^{-1/4} \frac{h}{a} \right]^2 \quad (5)$$

$$G_I = A(\eta) \frac{(Pa)^2}{E_1 h^3} \left[1 + Y_I(\rho)(1 + F_I(\rho)(1 - \eta))\lambda^{-1/4} \frac{h}{a} \right]^2 \quad (6)$$

$$G_{II} = G - G_I \quad (7)$$

where,

$$Y(\rho) = 0.484 + 0.122(\rho - 1) - 0.016(\rho - 1)^2 + 0.002(\rho - 1)^3$$

$$Y_I(\rho) = 0.677 + 0.146(\rho - 1) - 0.0178(\rho - 1)^2 + 0.00242(\rho - 1)^3$$

$$F(\rho) = 0.468 \exp(-0.181\sqrt{\rho})$$

$$F_I(\rho) = 0.5185 - 0.0244\rho$$

$$A(\eta) = 3.734 - 0.223\eta - 0.867\eta^2 + 0.356\eta^3$$

$$\lambda = \frac{E_2}{E_1}$$

$$\rho = \frac{(E_1 E_2)^{1/2}}{2G_{12}} - (v_{12} v_{21})^{1/2}$$

In order to confirm the validity of J-integral used in this study, J-integral values computed through ABAQUS were compared with the energy release rates computed using VCCT^[5,9] through ABAQUS.

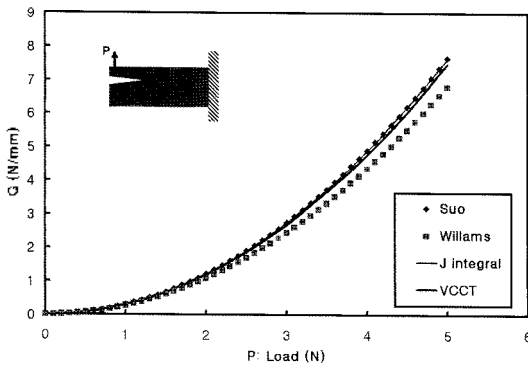


Fig. 5. Comparison among VCCT and J-integral computed through ABAQUS and the energy release rates derived by Suo and Williams.

Also, J-integral values are compared with the energy release rates predicted by Suo *et al.*^[4] and the energy release rates derived by Williams^[11]. The comparisons are shown in Fig. 5. Using the mixed mode End-Loaded-Split geometry (Fig. 4) made of an isotropic material (Goodrich Epoxy Adhesive; $E=3.720\text{GPa}$, $\nu=0.34$), the energy release rates are calculated. In equation (5), (6), (7) derived by Suo, $\lambda=\rho=1$ for an isotropic material. As seen in Fig. 5, J-integral based computation through ABAQUS shows excellent agreement with G computed through VCCT via ABAQUS and G derived by Suo, while there is a discrepancy between G derived by Williams and G computed through VCCT via ABAQUS. Thus, the energy release rate expression derived by Williams is erroneous.

2.3 Numerical Modeling

A numerical model which is a half of a typical bonded test panel is shown in Fig. 6. The finite element model contains 3983 elements. These elements are 6-node quadratic plane strain triangular elements

(CPE6 elements in ABAQUS) and 8-node biquadratic plane strain quadrilateral elements (CPE8 elements in ABAQUS).

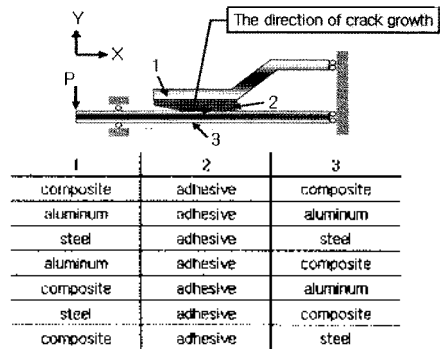


Fig. 6. The geometry of a structure studied here and 7 combinations of materials applied to the structure.

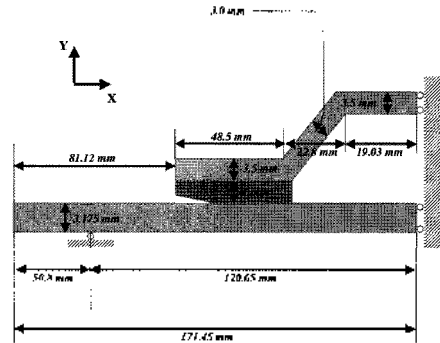


Fig. 7. The dimensions of the structure.

To perform a J-integral analysis via ABAQUS, second-order elements must be used and the elements around the crack tip in the numerical model must be collapsed using node collapsing^[13]. As seen in Fig. 6, we studied 7 cases through the numerical analysis via ABAQUS. Each case has different combinations of materials, respectively. The dimensions of the specimen in Fig. 6 are shown in Fig. 7.

3. Numerical Results

For each combination of materials (hat section, adhesive and substrate, see Fig. 6), the numerical analyses are performed using elastic and plastic property of the adhesive material and elastic properties of the materials for the hat and substrate sections. In the analyses of the structure, properties of the adhesive material measured ($E=3.720\text{GPa}$, $\nu=0.34$) were used.

Fig. 8 shows J integral values corresponding to crack opening obtained via three different analyses under load control.

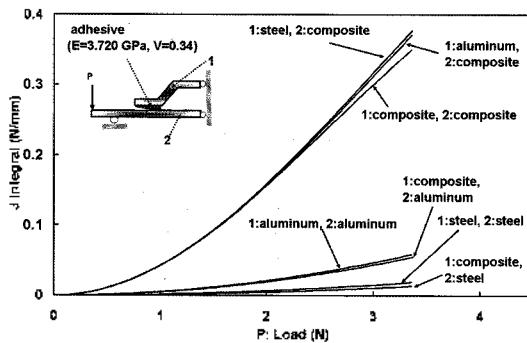


Fig. 8. J integral of crack opening for 7 combinations of materials in the hat stiffened structure.

Fig. 8 shows variations of J integral as a function of increase of load on the structure. In the analyses corresponding to crack opening under load control (see Fig. 8), the J integral values for a *steel (hat section) & composite (substrate)* are the highest, although the J integral values for a *steel (hat section) & composite (substrate)* has a similar value to *aluminum (hat section) & composite (substrate)* and *composite (hat section) & composite (substrate)*.

Table 3. Rank of 7 different material combinations in the hat stiffened structure in terms of the J integral

Rank	Structure
1 st	steel (hat) & composite (substrate)
2 nd	aluminum (hat) & composite (substrate)
3 rd	composite (hat) & composite (substrate)
4 th	aluminum (hat) & aluminum (substrate)
5 th	composite (hat) & aluminum (substrate)
6 th	steel (hat) & steel (substrate)
7 th	composite (hat) & steel (substrate)

The rank of different structures in terms of the J integral values corresponding to crack closing under load control is the same as the rank related to crack opening. From Fig. 8, we can rank 7 different structures containing 7 different combinations of materials, in terms of the J integral values as shown in Table 3.

4. Discussions

To understand the variations of the J integral values

under load control, Fig. 9 has been constructed.

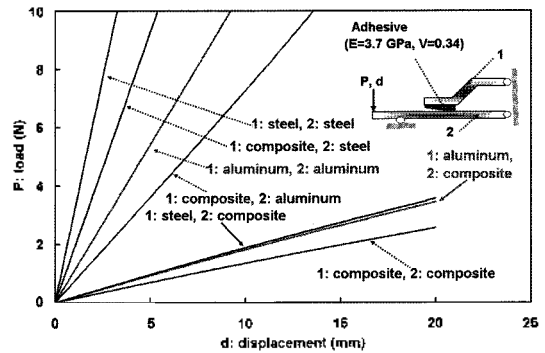


Fig. 9. The load-displacement responses of the structure.

Fig. 9 shows load-displacement responses of 7 configurations containing 7 different combinations of materials, respectively. In this Fig., the structure having *composite (hat section) & composite (substrate)*, experiences the largest displacement to reach a certain load, while the structure having *steel (hat section) & steel (substrate)* experiences the least displacement to reach the load. Hence, we can rank these different structures, in terms of the structural compliance as shown in Table 4. The use of a composite material for the hat and the substrate sections of the structure, as seen in Fig. 6, is the worst choice to initiate crack propagation because nonlinear effects such as nonlinear geometry due to large deformation and nonlinear material properties (plastic properties) are involved.

Table 4. Rank of 7 different structures in terms of the compliance of crack opening

Rank	Structure
1 st	composite (hat) & composite (substrate)
2 nd	aluminum (hat) & composite (substrate)
3 rd	steel (hat) & composite (substrate)
4 th	composite (hat) & aluminum (substrate)
5 th	aluminum (hat) & aluminum (substrate)
6 th	composite (hat) & steel (substrate)
7 th	steel (hat) & steel (substrate)

The best choice to initiate crack propagation of the structure is the structure with *steel (hat section) & steel (substrate section)* because the structure can reach the critical value of J to initiate crack propagation in the linear regime of the structural response

without involving the above nonlinear effects.

Table 5. Rank of 7 different structures in terms of the ease to initiate crack propagation based on a critical J_{total}

Rank	Structure
1 st	steel (hat) & steel (substrate)
2 nd	composite (hat) & steel (substrate)
3 rd	aluminum (hat) & aluminum (substrate)
4 th	composite (hat) & aluminum (substrate)
5 th	steel (hat) & composite (substrate)
6 th	aluminum (hat) & composite (substrate)
7 th	composite (hat) & composite (substrate)

Also, the structure with *composite (hat section) & steel (substrate)* is easier to initiate crack propagation than the structure with *steel (hat section) & composite (substrate section)*. This is caused by less difference of material properties between the adhesive and the substrate structure subjected to the external load. Hence, we can rank 7 different structures containing 7 different combinations of materials respectively, in terms of ease to initiate crack propagation as shown in Table 5.

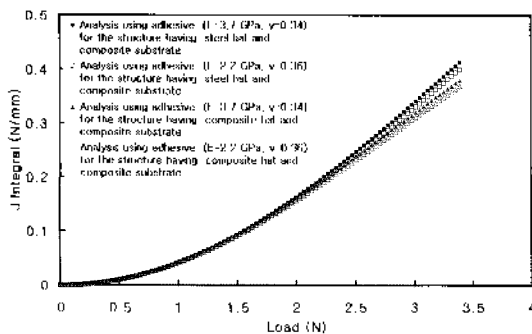


Fig. 10. Comparison of J integrals on the influence of the adhesive material in the structure.

The influences of the adhesive material properties on the J-integral value for the structure using *steel (hat section) & composite (substrate)* and *composite (hat section) & composite (substrate)* are shown in Fig. 10. Two different cases of the adhesive material were compared. One is $E=2,168$ GPa, $\nu=0.36$ ^[2] and the other is $E=3,720$ GPa, $\nu=0.34$ (measured properties). As seen in Fig. 10, J-integral values of the structure for two different properties of the adhesive material are similar despite the big discrepancy

between the properties. Hence, it is concluded that the adhesive material properties do not influence the computations of the J-integral values whereas the material properties of the hat and the substrate sections have a more important role in influencing the J-integral value associated with the structure.

6. Conclusions

In this paper, it has been studied what kind of material combinations causes the easier crack initiation in the bonded hat section/substrate structures structure among 7 kinds of material combinations. The conclusions through this study are as follows.

(1) The best choice to initiate crack propagation of the structure is the structure with *steel (hat section) & steel (substrate section)*.

(2) The structure with *composite (hat section) & steel (substrate)* is easier to initiate crack propagation than the structure with *steel (hat section) & composite (substrate section)*.

(3) The adhesive material properties do not influence the computations of the J-integral values too much when compared to the material properties of the hat and the substrate sections.

Acknowledgements

The author wishes to thank to Prof. A. M. Waas in the University of Michigan at Ann Arbor for providing valuable suggestions and advices.

References

1. Fernlund, G. and Spelt, J. K., "Mixed-mode Fracture Characterization of Adhesive Joints", *Composite Science and Technology*, Vol. 50, No. 44, pp. 441-449, 1994.
2. Fernlund, G. and Spelt, J. K., "Failure Load Prediction of Structural Adhesive Joints: Part 1. Analytical Method", *Int. J. Adhesion and Adhesives*, Vol. 11, pp. 213-220, 1991.
3. Suo, Z. and Hutchinson, J. W., "Interface Crack Between Two Elastic Layers", *Int. J. of Fracture*, Vol. 43, No. 1, pp. 1-18, 1990.
4. Bao, G., Ho, S., Fan, B. and Suo, Z., "The Role of Material Orthotropy in Fracture Specimens for Composites", *Int. J. Solids & Structures*, Vol. 29, No. 9, pp. 1105-1116, 1992.
5. Shen, F., Lee, K. H. and Tay, T. F., "Modeling Delamination Growth in Laminated Composites",

- Composite Science and Technology*, Vol. 61, No. 9, pp. 1239-1251, 2001.
6. Johnson, M. J. and Sridharan, S., "Evaluation of Strain Energy Release Rates in Delaminated Laminates Under Compression", *AIAA Journal*, Vol. 37, No. 8, pp. 954-963, 1999.
 7. Sridharan, S., "Displacement-based Mode Separation of Strain Energy Release Rates for Interfacial Cracks in bi-material Media", *Int. J. Solids & Structures*, Vol.38, No. 38, pp. 6787-6803, 2001.
 8. Tay, T. E., Shen, F., Lee, K. H., Scaglione, A. and Di, S. M., "Mesh Design in Finite Element Analysis of Post-buckled Delamination in Composite Laminates", *Composite Struct.*, Vol. 47, No. 1, pp. 603-611, 1999.
 9. Xie, D., Chung, J., Waas, A. M., Shahwan, K. W., Schroeder, J. A., Boeman, R. G., Kunc, V. and Klett, L. B., "Failure Analysis of Adhesively Bonded Structures: From Coupon Level Data to Structural Level Predictions and Verification", *Int. J. Fract.*, Vol. 134, pp. 231-250, 2005.
 10. Reeder, J. R. and Crews, J. H. Jr., "Mixed-mode Bending Method for Delamination Testing", *AIAA Journal*, Vol. 28, No. 7, pp. 1270-1276, 1990.
 11. J. G. Williams, "On the Calculation of Energy Release Rates for Cracked Laminates", *Int. J. Fract.*, Vol. 36, pp. 101-119, 1988.
 12. Morman, K. N. and Shahwan, K. W., "3-dimensional Elastic Finite Element Fracture Analysis of Cohesive and Interfacial Planar Cracks in a Prototypical Composite Adherend/epoxy Adhesive Bonded Joint", *Final Report, Vehicle Safety*. Research Department, Ford Research Laboratories, 1997.
 13. Pilkey, W. D., "Formulas for Stress, Strain and Structural Matrices", *John Wiley & Sons, Inc.*, 1994.
 14. ASM Specialty Handbook, "Aluminum and Aluminum Alloys", *ASM International*.
 15. ABAQUS/STANDARD, User's Manual, Version 6.7, Vol. I, II and III,, *Hibbitt, Karlsson & Sorensen, Inc.*, 2007.

정 재 응



1987년 성균관대학교 기계설계학과 학사
 1997년 The Univ. of Michigan 항공
 공학 석사
 2000년 The Univ. of Michigan 항공
 공학 박사
 2001년~2002년 The Univ. of Michigan
 Research Fellow
 2003년~2006년 현대·기아자동차연
 구개발본부 선임연구원
 2006년~현재 경원대학교 기계자동차
 공학과 조교수
 관심분야: Numerical Analysis and
 Experiments for Mechanical and
 Aerospace structures, 복합재료 및
 벌집구조체 거동 특성, 문화 콘텐츠
 츠 기술
